THE JOURNAL OF NAVIGATION (2005), **58**, 119–134. © The Royal Institute of Navigation
DOI: 10.1017/S0373463304003005 Printed in the United Kingdom

Wavelet Analysis For Improving INS and INS/DGPS Navigation Accuracy

Sameh Nassar and Naser El-Sheimy

(*The University of Calgary*)
(Email: naser@geomatics.ucalgary.ca)

The integration of the Global Positioning System (DGPS) with an Inertial Navigation System (INS) has been implemented for several years. In an integrated INS/DGPS system, the DGPS provides positions while the INS provides attitudes. In case of DGPS outages (signal blockages), the INS is used for positioning until the DGPS signals are available again. One of the major issues that limit the INS accuracy, as a stand-alone navigation system, is the level of sensor noise. The problem with inertial data is that the required signal is buried into a large window of high frequency noise. If such noise component could be removed, the overall inertial navigation accuracy is expected to improve considerably. The INS sensor outputs contain actual vehicle motion and sensor noise. Therefore, the resulting position errors are proportional to the existing sensor noise and vehicle vibrations. In this paper, wavelet techniques are applied for de-noising the inertial measurements to minimize the undesirable effects of sensor noise and other disturbances. To test the efficiency of inertial data de-noising, two road vehicle INS/DGPS data sets are utilized. Compared to the obtained position errors using the original inertial measurements, the results showed that the positioning performance using de-noised data improves by 34%–63%.

KEY WORDS

1. DGPS. 2. INS. 3. Inertial Sensor Noise. 4. Wavelets.

1. INTRODUCTION. The last two decades have shown an increasing trend in using integrated INS/DGPS systems in many applications requiring position and attitude information. For example in mobile mapping systems, the INS/DGPS navigation information (position and attitude) is used to georeference an imaging sensor mounted on the same carrier of the integrated INS/DGPS system. Another application of INS/DGPS that has received the attention of geodesists in the last decade is airborne gravimetry. Using the INS/DGPS navigation solution and subtracting the aircraft acceleration (obtained by twice differentiating DGPS positions) and the total sensed acceleration (obtained by INS accelerometer specific force measurements), the gravity field can be determined with high accuracy. In general, GPS provides highly accurate position and velocity and can provide attitude information when a multi-antenna system is used. However, GPS is not suitable enough for many mapping and navigation applications that require continuous navigation information (Schwarz and Wei, 1995). Cycle slips caused by loss of lock between the receiver and a satellite are one of the limitations of GPS. In addition, some

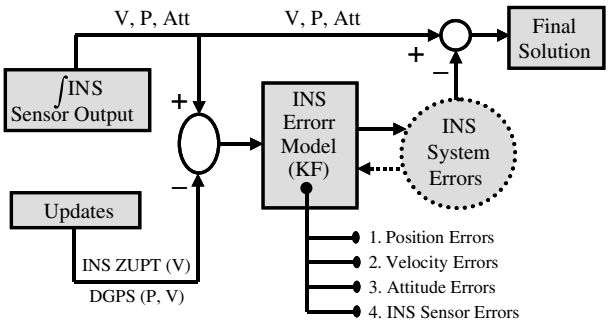

Figure 1. INS Stand-Alone and INS/DGPS Integration Schemes.

applications require a very high data rate (e.g. 100–200 Hz), which cannot be provided by current GPS receivers. This means that the GPS cannot sense dynamic changes rapidly enough for some applications.

On the other hand, INS is a self-contained system, which in the short term, provides accurate position, velocity and attitude information at a very high data rate (generally above 50 Hz), but has time dependent error growth when operated in a stand-alone mode. Therefore, the two systems are complementary. In an integrated INS/DGPS system, the primary function of the DGPS is to provide position information while the primary function of the INS is to provide attitude information. In addition, the short-term position accuracy of the INS can be used to detect and correct cycle slip problems in the GPS carrier phase data. Finally, the DGPS can be used for the in-motion calibration of inertial sensors, while the INS can be used for positioning during DGPS outages.

In the standard operation of INS stand-alone navigation and INS/DGPS integration applications, the dynamic behavior of the INS is described using a system of differential equations and then kinematic measurements are used to solve it to provide positions, velocities and attitudes. Due to the INS sensor errors, the solution of such system of differential equations contains errors. Therefore, these errors are determined first through error models and then compensation for them is performed through a Kalman Filter (KF), see Figure 1. The updates for the KF in INS stand-alone positioning are Zero Velocity Update (ZUPT) measurements while in INS/DGPS integration mode, the updates are the DGPS position and velocity. One of the major problems that can affect the overall INS/DGPS integrated system accuracy is the existence of frequent DGPS outage periods that are caused by GPS signal blockages. As a solution to the positioning problem during DGPS outages, just the INS is used for positioning without any updates until the GPS signal is re-acquired with sufficient accuracy. This mode of INS stand-alone positioning is essentially a prediction process. Thus, the solution accuracy in such situations is mainly governed by the inertial system errors.

However, it is a well-known fact in inertial navigation that all gyro and accelerometer technologies suffer from relatively high measurement noise. The noise affecting inertial sensors contains two parts: a low frequency component and a high frequency component. Both components are combined together and affect the inertial sensor measurement accuracy. The high frequency component has white noise

characteristics while the low frequency component is characterized by correlated noise. The correlated noise can be modelled with sufficient accuracy using random process error models whereas the white noise part cannot. In inertial navigation applications, the useful INS sensor signals (accelerometer specific forces and gyro angular rates) are hidden in high frequency (white noise) measurement noise. Therefore, if such white noise component could be separated (or removed) from the measured inertial sensor signal, the performance of inertial measurements is expected to improve. In turn, the overall INS accuracy will be improved. The separation of the high frequency noise components can be performed by de-noising the inertial measurements.

De-noising of INS sensor measurements using wavelet decomposition is presented in this paper as an effective method to cope with inertial sensor noise in INS stand-alone navigation and INS/DGPS integration applications. In INS/DGPS kinematic applications, de-noising of INS data signals by wavelet decomposition techniques has been successfully used in considerably reducing estimated attitude errors; see Ŝkaloud (1999) for more details. It also has been used to improve the estimation of airborne gravity disturbance values, using INS data de-noised by wavelets, see Bruton et al. (2000) for details. However in this case, the improvement was rather minimal. Since the INS sensor outputs contain effects of actual vehicle motion and sensor noise, the resulting position errors will be proportional to the existing inertial sensor noise and vehicle vibrations. Wavelet techniques can be applied for removing the high frequency noise in order to minimize the undesirable effects of sensor noise and other high frequency disturbances. In such situations, it is expected that the position errors obtained from de-noised INS data will be smaller than the ones obtained from the original data.

In this paper, the Wavelet Transform (WT) will be presented first. After that, the principle of wavelet multi-resolution analysis (multiple levels of wavelet decomposition) will be introduced and then discussed considering both static and kinematic mode situations. The effect of de-noising INS kinematic data will be analyzed after comparing the obtained position errors, using both the original and the de-noised INS data in kinematic stand-alone INS navigation and INS/DGPS integration with some simulated DGPS outages. For this purpose, two kinematic road vehicle data sets collected using two Inertial Measurement Units (IMUs) of high and medium accuracy will be utilized. Finally, the obtained results are discussed and some conclusions are drawn.

2. WAVELETS AND THE WAVELET TRANSFORM (WT).

Wavelets have received extensive attention in the engineering profession during the last two decades. From the mid-1980s till now, wavelet techniques have been implemented in many applications such as: image processing, medical diagnostics, geophysical signal processing, pattern recognition, electromagnetic wave scattering, boundary value problems, … etc. (Goswami and Chan, 1999). Wavelet techniques are based on analyzing a signal through signal windowing but with variable window sizes. This gives an advantage to wavelets over other signal processing techniques in that it is capable of performing local analyses, i.e. analyzing a localized portion of a large signal (Polikar, 1996). This is possible since wavelets allow the use of narrow windows (short-time intervals) if high frequency information is

Symlets (sym8) Daubechies (db2) Coiflets (coif1) Daubechies (db8)

Figure 2. Examples of Some Existing Mother Wavelets (Misiti et al., 2000).

needed and wide windows (long-time intervals) if low frequency information is required.

2.1. *The Continuous Wavelet Transform.* The Continuous Wavelet Transform (CWT) $\mathbf{X}^C_{\mu,\nu}$ of a continuous-time domain signal $\mathbf{x}(t)$ is defined as the inner product of the signal sequence with a family of functions $\psi_{\mu,\nu}(t)$, such as:

$$\begin{aligned}\mathbf{X}^C_{\mu,\nu} &= \langle \mathbf{x}(t), \psi_{\mu,\nu}(t) \rangle \\ &= \int_{-\infty}^{\infty} \mathbf{x}(t)\, \psi^*_{\mu,\nu}(t)\, dt\end{aligned} \tag{1a}$$

where the * indicates complex conjugation and the family $\psi_{\mu,\nu}(t)$ is defined by continuous scaling (dilation or compression) parameters μ and translation parameters ν of a single analyzing function $\psi(t)$ such that:

$$\psi_{\mu,\nu}(t) = \frac{1}{\sqrt{\mu}}\, \psi\left(\frac{\mathrm{t}-\nu}{\mu}\right), \qquad \mu > 0 \tag{1b}$$

Substituting Equation 1b into Equation 1a, we obtain:

$$\mathbf{X}^C_{\mu,\nu} = \frac{1}{\sqrt{\mu}} \int_{-\infty}^{\infty} \mathbf{x}(t)\ \psi^*\left(\frac{\mathrm{t}-\nu}{\mu}\right) dt \tag{1c}$$

Therefore, the wavelet transformation of a time-domain signal, in general, is defined in terms of the projections of this signal onto a family of basis functions that are generated by dilations (or compressions) and translations of a single function. The single analyzing function is called the "mother or prototype wavelet" while the basis functions are called "daughter wavelets". Two conditions must be satisfied for ψ to be a window function and also to give the ability to recover (or reconstruct) the signal $\mathbf{x}(t)$ from $\mathbf{X}^C_{\mu,\nu}$. The first condition is that ψ must be short and the second one is that it must be oscillatory, i.e. ψ must have zero-mean and decay quickly at both ends (Strang and Nguyen, 1996; Goswami and Chan, 1999; Keller, 2000). Figure 2 shows some examples of existing mother wavelets that satisfy the above two conditions.

Wavelets offer the capability of detecting variable frequency components in a signal as well as the time of their existence. This is obtained through the dilation and translation parameters μ and ν (Goswami and Chan, 1999). In Equation 1c, by changing the value of μ in $\psi^*\left(\frac{\mathrm{t}-\nu}{\mu}\right)$, the time (or window) support of $\psi_{\mu,\nu}$ will also

https://doi.org/10.1017/S0373463304003005 Published online by Cambridge University Press

be changing. In other words, if μ is reduced, the time window of $\psi_{\mu,\nu}(t)$ will narrow, and thus, high-frequency information could be detected. The opposite is true when μ is increased. Therefore, the parameter $1/\mu$ is a measure of frequency and hence μ can be considered as a "scale" that determines the oscillating behavior of a particular daughter wavelet $\psi_{\mu,\nu}(t)$. On the other hand, the translation parameter ν indicates the time location of the wavelet window (i.e. the "shift" of the wavelet along the time axis), which provides the time localization information of the original signal.

From Equation 1c, if the signal at one of its locations has a spectral component that is closely related to the current value of the scale μ, the computed coefficient at this point will have a relatively large value, and vice versa (Polikar, 1996; Mallat, 1998). The computation of the CWT coefficients starts at the beginning of the signal using the most compressed wavelet that can detect the highest frequencies existing in the signal. This is performed by choosing a scale value that represents the original signal. Then, the wavelet is shifted by ν along the time axis until the end of the signal. The next step is to increase the scale μ by some amount (thus expanding the wavelet window to detect lower frequencies) and repeat the shifting procedure. The whole procedure is repeated for each value of μ until some "maximum" desired value of μ is reached.

2.2. *The Discrete Wavelet Transform.* Since inertial sensor signals are discrete-time signals, the Discrete Wavelet Transform (DWT) is implemented instead of the CWT. In this case, the basis functions are obtained by discretizing (sampling) the continuous parameters μ and ν. In the DWT, the sampling of μ and ν is based on powers of some constant number α and it takes the form:

$$\mu = \alpha^n \tag{3a}$$

$$\nu = m\alpha^n \tag{3b}$$

where n and m are integer numbers representing the discrete dilation and translation indices. Moreover, and from the practical aspects of the wavelet theory analysis, it has been found that the most efficient way of determining μ and ν is the "dyadic" one, i.e. to take the value of α to be 2. By substituting Equations 3 into Equation 1c, the CWT will take the form:

$$\mathbf{X}^C_{\mu,\nu} = \frac{1}{\sqrt{\alpha^n}} \int_{-\infty}^{\infty} \mathbf{x}(t)\ \psi(t\alpha^{-n} - m)dt \tag{4}$$

Then, by discretizing $\mathbf{x}(t)$ to $\mathbf{x}(k)$ assuming a sampling rate of 1 (i.e. $k = t$) and considering $\alpha = 2$, the DWT $\mathbf{X}^D_{n,m}$ of a discrete-time signal $\mathbf{x}(k)$ can be described by the two integers n and m as:

$$\mathbf{X}^D_{n,m} = \frac{1}{\sqrt{2^n}} \sum_k \mathbf{x}(k)\ \psi(k2^{-n} - m) \tag{5}$$

For many signals (especially INS sensor data), the low frequency component of the signal is the one of interest since it gives the identity of such signal. On the other hand, the high frequency component usually constitutes the signal noise. In wavelet terminology, the low frequency component of a signal is called the "approximation part" while the high frequency component is called the "details part". In the

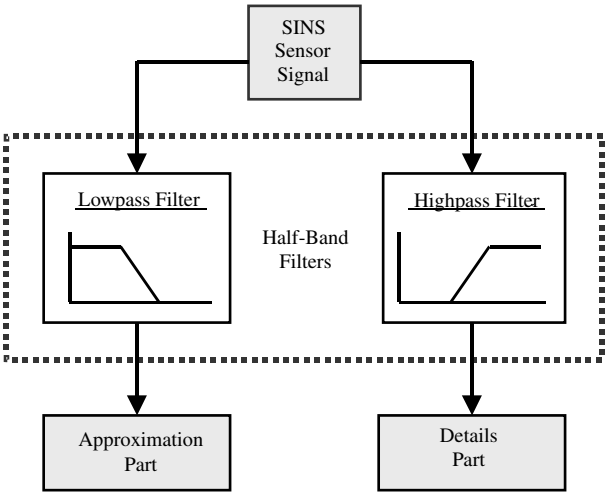

Figure 3. Signal Decomposition by the Discrete Wavelet Transform (DWT).

implementation of the DWT, the wavelet coefficients of a signal are computed by passing such a signal through two complementary half-band filters: a Low-Pass (LP) filter and a High-Pass (HP) filter. Therefore, the input signal in case of implementing the DWT will be decomposed into two parts. The first part will be the output of the HP filter (i.e. the details) while the second part will be the output of the LP filter (i.e. the approximation), see Figure 3.

In the above discussion, it has been shown how the DWT can be used to analyze (or decompose) a signal into its approximation and details components. However, as in any application that involves transforming a signal from its time-domain to another domain, the requirement after that is the reconstruction of the signal back into its original domain without loosing any information. Basically, in the case of wavelets, this will be obtained by applying the Inverse Discrete Wavelet Transform (IDWT) on the previously computed wavelet coefficients. To reconstruct a signal from its wavelet coefficients, the approximation and details coefficients are passed separately through another LP and HP filters. The decomposition LP and HP filters and the associated reconstruction LP and HP filters are not identical but are closely related, and they form a known system in the signal processing literature that is called "quadrature mirror filters" (Misiti et al., 2000). For more details about the design of the decomposition and the corresponding reconstruction LP and HP filters, see Strang and Nguyen (1996).

3. WAVELET MULTI-RESOLUTION ANALYSIS.

Based on the Nyquist theorem, if a signal has a sampling frequency of f_s, the highest frequency component that the signal would represent is $f_s/2$ (Oppenheim and Schafer, 1999). By applying the DWT to decompose a signal and recalling that the LP and HP filters (shown in the filter bank of Figure 3) have half-band characteristics, then the cutoff frequency of the LP filter is exactly at one half of the maximum frequency appearing at the signal. Hence, if the DWT is applied on an inertial data of

https://doi.org/10.1017/S0373463304003005 Published online by Cambridge University Press

sampling frequency f_s, the approximation part will include those inertial signal components that have frequencies of less than $f_s/2$ while the details part will include the components of frequencies between $f_s/4$ and $f_s/2$. To obtain the lower resolution frequency components (i.e. that are less than $f_s/4$), the approximation part can be decomposed using the same process into two other approximation and details components. In this case, the second approximation part will include all frequency components of less than $f_s/8$ while the second details part will include frequencies between $f_s/8$ and $f_s/4$.

Therefore, to obtain finer resolution frequency components of a specific signal, the signal is broken down into many lower-resolution components by repeating the DWT decomposition procedure with successive decompositions of the obtained approximation parts. This procedure is called either wavelet multi-resolution analysis or wavelet multiple Level of Decomposition (LOD). However, this capability of representing a signal at several levels of resolution constitutes one of the major powerful facilities of wavelets over other signal processing techniques. Using wavelet multi-resolution analysis, the signal can be represented by a finite sum of components at different resolutions, and hence, each component can be processed adaptively depending on the application at hand (Goswami and Chan, 1999). As mentioned before, the signal is reconstructed by applying the IDWT on its computed wavelet coefficients. Using wavelet multi-resolution analysis, the inertial sensor signal can be represented as:

$$\begin{aligned}\text{Inertial Signal} &= A_1 + D_1 \\ &= A_2 + D_2 + D_1 \\ &= A_3 + D_3 + D_2 + D_1 \\ &= A_n + D_n + D_{n-1} + \ldots + D_1 \end{aligned} \tag{6}$$

where A and D represent the signal approximation and details components, respectively, and $n = 1, 2, 3 \ldots$ is the wavelet LOD. Since the application at hand is INS sensor data de-noising, the desired reconstructed signal is obtained by passing the coefficients of the selected approximation level through the IDWT LP filter and resetting the coefficients of all subsequent details to zero before passing them through the IDWT HP filters.

4. SELECTION OF THE APPROPRIATE WAVELET LEVEL OF DECOMPOSITION.

In theory, the wavelet decomposition process of a signal can be continued indefinitely, but in reality it can be performed only until the individual details consist of a single sample. Practically, an appropriate Level of Decomposition (LOD) is chosen based on the nature of the signal or on a specific criterion (Misiti et al., 2000). In our case of INS sensor data, we have two modes of operation: static and kinematic. For both operation modes, the selection of an appropriate LOD is based on removing the high-frequency noise but keeping all the useful information contained in the signal. For static inertial data, the sensors outputs contain the following signals: the Earth gravity components, the Earth rotation rate components and the sensors long-term errors (such as biases). These signals have very low frequency, and hence, they can be separated easily from the high frequency noise components by the wavelet multi-resolution analysis. To select

https://doi.org/10.1017/S0373463304003005 Published online by Cambridge University Press

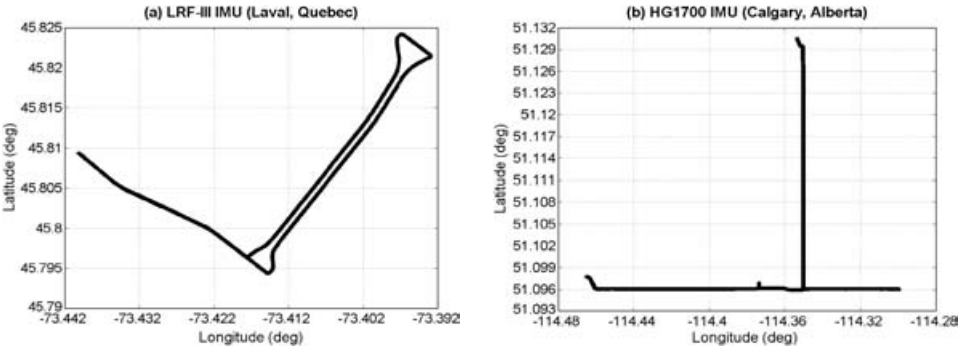

Figure 4. INS/DGPS Van Test Trajectories.

an appropriate LOD in this case, several decomposition levels are applied and the Standard Deviation (STD) is computed for each obtained approximation component. As shown in Nassar et al. (2003), the proper LOD will be the one after which the STD reaches its minimum value.

In case of kinematic inertial data de-noising, the output of the sensors contains both effects of the actual vehicle motion dynamics and the sensor noise as well as some other undesirable effects (e.g. vehicle engine vibrations). Therefore, the criterion for the selection of the appropriate LOD will be different from the static data case. Before applying the wavelet multi-resolution analysis on kinematic INS data, it should be ensured that the decomposition or de-noising process does not remove any actual motion information. To satisfy this condition, a spectral analysis of the used kinematic INS sensor raw data should be performed first. In Geomatics engineering of airborne, shipborne and land vehicle applications, the vehicle motion dynamics is usually in the low frequency portion of the spectrum. Therefore, by analyzing the raw data in the frequency domain, the low frequency range of the actual vehicle motion can be detected. Then, the appropriate LOD can be selected in such a way that the decomposition process will remove only the components that have frequencies higher than the detected motion frequency range.

5. KINEMATIC INS AND INS/DGPS DATA TESTING USING DE-NOISED INS DATA.

To test the effect of de-noising inertial sensor data on the system results, the positioning performance of INS stand-alone navigation or INS/DGPS integration during DGPS outages is analyzed using two van data sets. The first data set was collected in Laval, Québec using Ashtech Z12 GPS receivers and a navigation-grade (gyro drift of 0·005–0·01 deg/h) IMU (Honeywell LRF-III) while the second test was performed in Calgary, Alberta using NovAtel OEM4 GPS receivers and a tactical-grade (gyro drift of 1·0–10·0 deg/h) IMU (Honeywell HG1700). The two van test trajectories are shown in Figure 4 while the characteristics of both tests are summarized in Table 1.

For both data sets, a spectral analysis is performed first for the original INS raw data to choose the appropriate wavelet LOD that removes only the undesirable sensor noise and other vibrations and also maintains the actual motion dynamics.

https://doi.org/10.1017/S0373463304003005 Published online by Cambridge University Press

Table 1. Summary of the Performed INS/DGPS Kinematic Tests.

Kinematic Test	Laval, Québec LRF-III IMU	Calgary, Alberta HG1700 IMU
Static Initialization Time (minute)	15	18
Average Van Speed (km/h)	50	65
Number of Performed ZUPTs	19	35
Minimum Number of Available Satellites	7	5
Average Number of Available Satellites	8	6
Average PDOP	1·5	1·8
Maximum Rover-Master Distance (km)	4·0	6·0
GPS Data Rate (Hz)	1·0	1·0
SINS Data Rate (Hz)	50	100

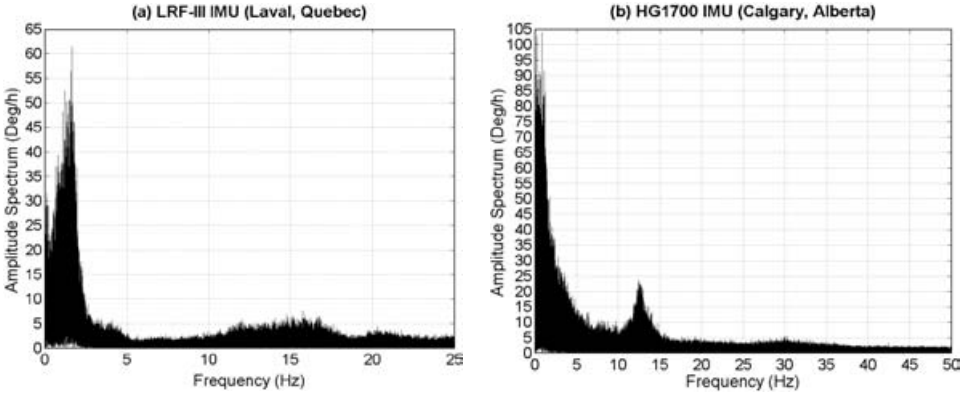

Figure 5. The Spectrum of One Gyro of Each Van Kinematic Data.

As mentioned before, the maximum frequency that can appear at the INS raw signal is $f_s/2$, where f_s is the data sampling frequency (data rate in Hz). The data rates of the used IMUs are 50 Hz for the LRF-III and 100 Hz for the HG1700. Therefore, the data highest visible frequency will be 25 Hz for the first data set and 50 Hz for the second data set, respectively. To show the performed spectral analysis, the spectrum of one set of sensor data from each test is shown. For the rest of the two IMU sensors, the spectrum characteristics are quite similar. Figure 5 shows the spectrum of one of the used gyros for each IMU. The figures clearly indicate that the bandwidth that contains the majority of the motion dynamics for both tests falls in the low frequency portion of the spectrum with a cutoff frequency, somewhat below 3 Hz.

However, a peak in the amplitude spectrum between 11 Hz and 13 Hz is observed in Figure 5b (HG1700 gyro). This is most probably due to the van engine vibrations, i.e. it is considered as undesirable noise in terms of motion detection. To check this assumption, a spectral analysis for the gyro alignment static data is performed since the van engine was on during the initial alignment period. The obtained spectrum for the static data is shown in Figure 6. The figure shows a peak that is similar to the one obtained in Figure 5b with the same magnitude and same frequency band. This

https://doi.org/10.1017/S0373463304003005 Published online by Cambridge University Press

Table 2. Maximum Visible Frequency in Kinematic Inertial Data Before and After Successive Levels of Wavelet De-noising.

Type of Inertial Data	Maximum Frequency Appears in Data	Maximum Frequency Detected in Data (Hz)	
		Laval, Québec LRF-III IMU	HG1700 IMU Calgary, Alberta
Original Data	$f_s/2$	25	50
After Wavelet 1st LOD	$f_s/4$	12·5	25
After Wavelet 2nd LOD	$f_s/8$	6·25	12·5
After Wavelet 3rd LOD	$f_s/16$	3·125	6·25
After Wavelet 4th LOD	$f_s/32$	1·5625	3·125
After Wavelet 5th LOD	$f_s/64$	0·78125	1·5625

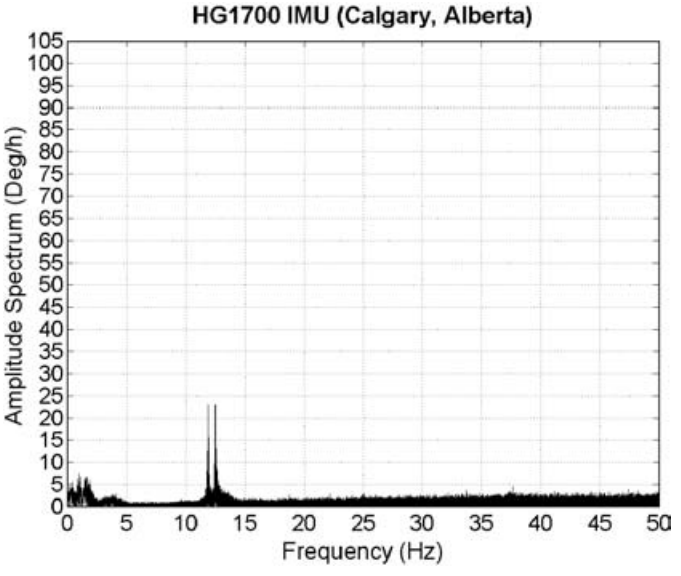

Figure 6. The Spectrum of One Gyro of Van Static Alignment Data.

confirms that engine vibration noise is the most likely cause for the peak in the spectrum.

For the selection of the proper wavelet LOD for each data set, the highest visible frequency values for both data sets after applying five successive levels of wavelet decomposition are computed and are listed in Table 2. From the figures in Table 2, the expected maximum wavelet LOD that can be applied safely in this case is level three for the LRF-III data and level four for the HG1700 data. This will remove any frequency component that is greater than 3·125 Hz. To show graphically the spectrum of the de-noised data, the LRF-III gyro data has been used. The spectra of the selected gyro for four levels of wavelet decomposition are shown in Figure 7. Figure 7d is compatible with the computations performed in Table 2 since it indicates that after applying the 4th LOD, some motion dynamics are removed from the required bandwidth and also the amplitude spectrum is reduced for the rest of the

https://doi.org/10.1017/S0373463304003005 Published online by Cambridge University Press

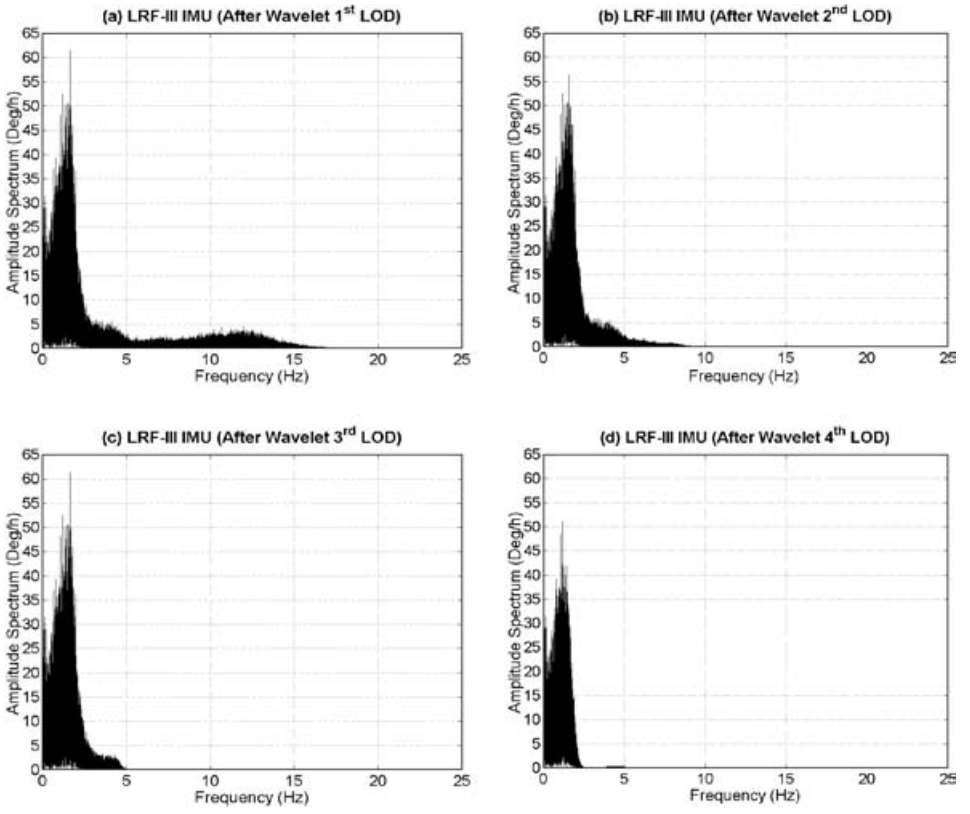

Figure 7. The Spectrum of LRF-III Gyro Data After Successive Wavelet Levels of Decomposition.

needed components. Similar results were obtained for the HG1700 gyro data after applying the 5th LOD.

To test the performance of inertial sensor data de-noising, two modes of processing are applied on both data sets. The first mode of processing is INS stand-alone positioning with frequent ZUPTs while the second mode of processing is INS/DGPS integration but with some intentionally induced DGPS outage periods. For each data set, the reference solution is obtained by processing the data in a complete INS/DGPS integration mode.

5.1. *Testing Wavelet De-noising with Stand-Alone INS.* Using INS stand-alone navigation with ZUPTs as updates, the position errors obtained using the original raw INS data (before de-noising) as well as the de-noised data with different wavelet LOD were computed. The statistics of such position errors are given in Table 3 while the position error Root Mean Square (RMS) values are shown in Figure 8. From Table 3 and Figure 8, it is clear that de-noising the INS sensor data by wavelet decomposition remarkably reduces the INS stand-alone position errors. Compared to the original data results, the LRF-III position errors (RMS) are decreased by 63% (using the 2nd LOD) while the HG1700 position errors (RMS) are decreased by 46% (using the 4th LOD). As expected, the obtained positioning errors start to get worse after applying decomposition levels that remove frequency components between

https://doi.org/10.1017/S0373463304003005 Published online by Cambridge University Press

Table 3. Stand-Alone INS Position Errors Before and After Wavelet De-noising of Inertial Data.

Kinematic Test	Type of Inertial Data	Error Statistics (m)		
		Mean	Max	RMS
Laval, Québec LRF-III IMU	Original Data	1·76	4·49	1·98
	After Wavelet 1st LOD	0·64	3·40	0·76
	After Wavelet 2nd LOD	0·58	3·16	0·73
	After Wavelet 3rd LOD	0·62	3·06	0·79
	After Wavelet 4th LOD	1·57	4·67	1·76
Calgary, Alberta HG1700 IMU	Original Data	43·72	148·78	53·11
	After Wavelet 1st LOD	37·83	138·55	46·70
	After Wavelet 2nd LOD	34·00	134·23	42·15
	After Wavelet 3rd LOD	24·48	132·25	29·98
	After Wavelet 4th LOD	24·19	130·51	28·91
	After Wavelet 5th LOD	32·69	218·52	38·57

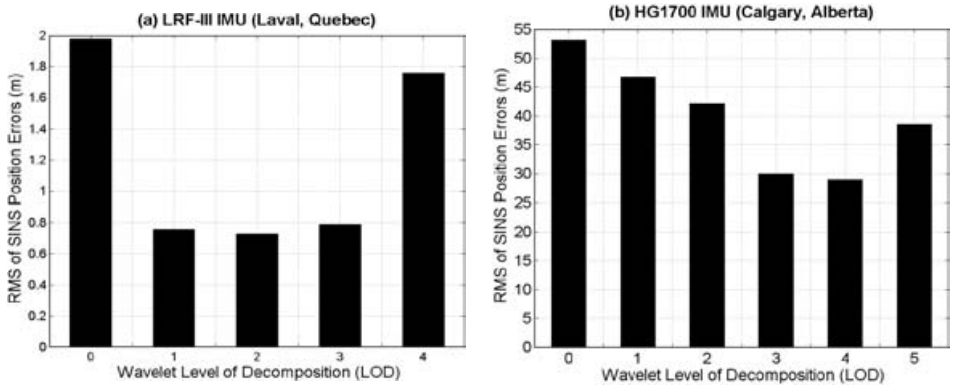

Figure 8. Stand-Alone INS Kinematic Position Errors Before and After Wavelet De-noising of Inertial Sensor Measurements.

1·5625 Hz and 3·125 Hz (4th LOD in case of LRF-III and 5th LOD in case of HG1700). Although the position errors after applying these decomposition levels are larger than those obtained from the previous levels, they are still better than the errors obtained from the original data. This can be explained by the fact that at this point, there is some kind of a compromise between removing additional noise and removing some motion information.

Moreover, and by examining the LRF-III test results, it can be seen that most of the improvement occurred just after applying the 1st LOD. This indicates in this case that the 1st LOD was capable of removing most of the undesirable noise in the LRF-III data. On the other hand, this is not the case for the HG1700 results where the improvement occurred gradually from the 1st LOD to the 4th LOD. This could be the result of two different causes. The first one is that the HG1700 is a tactical-grade IMU while the LRF-III is a navigation-grade IMU. Hence, the noise level (amplitude) of the HG1700 sensors is much larger, which in turn implies that more

https://doi.org/10.1017/S0373463304003005 Published online by Cambridge University Press

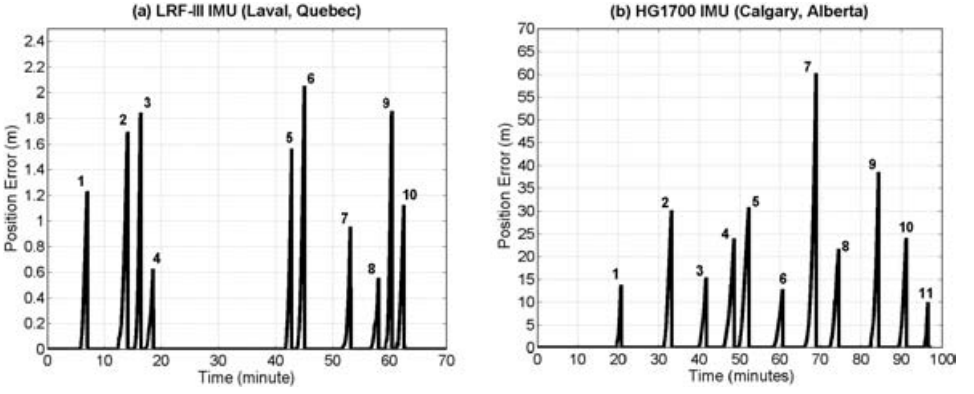

Figure 9. INS Position Errors During DGPS Outages (Before Inertial Data De-noising).

decomposition levels are required to remove or minimize the HG1700 noise. The second cause is that the HG1700 data rate (100 Hz) is higher than the LRF-III data rate (50 Hz), and thus, more decomposition levels are required to remove the high frequency components.

5.2. *Testing Wavelet De-noising with INS/DGPS.* For the first data set (LRF-III IMU), a total number of 10 DGPS outages were selected, while 11 outages were chosen for the second data set (HG1700 IMU). The selected outage intervals are ranged from 70 s to 100 s (LRF-III IMU) and from 70 s to 180 s (HG1700 IMU). The magnitude of the accumulated position errors during the selected DGPS outages of both data sets (before any inertial data de-noising) are computed and are shown in Figure 9.

The magnitude of position errors at the end of outage periods using the original and de-noised INS data are summarized in Table 4 while the average values of these errors are shown in Figure 10. These results agree with the obtained INS stand-alone results in Table 3 and Figure 8. During DGPS outages, using de-noised inertial data, the obtained position errors are improved by 34% in the case of the LRF-III data (using the 2nd LOD) and by 13% in case of the HG1700 data (using the 4th LOD).

However, it can be seen that the level of position error improvement in case of the INS/DGPS integration with DGPS outages is less than the corresponding improvement level in case of stand-alone INS navigation. This is due to the fact that the navigation mode and the type of available updates for INS only and INS/DGPS integration during DGPS outages are different. In INS stand-alone positioning, updates are available only through frequent ZUPTs, and hence navigation is performed in a prediction mode except at the ZUPT periods. Moreover, during any ZUPT interval, positioning errors are not reset to zero, and thus the obtained positioning errors are accumulated for the whole mission.

On the other hand, in INS/DGPS positioning, navigation is performed in a frequent update mode (using DGPS position and velocity updates) except at the DGPS outage intervals where prediction is utilized. Also, before and after any DGPS outage, positioning errors are reset almost to zero. Therefore, the obtained positioning errors during any outage are independent of the other outages (i.e. position errors

https://doi.org/10.1017/S0373463304003005 Published online by Cambridge University Press

Table 4. INS Position Errors During DGPS Outages Before and After Wavelet De-noising of Inertial Data.

Van Test	LRF-III IMU Errors (m) (Laval, Québec)						HG1700 IMU Errors (m) (Calgary, Alberta)						
Inertial Data Type	Outage No.	Original Errors	After 1st LOD	After 2nd LOD	After 3rd LOD	After 4th LOD	Outage No.	Original Errors	After 1st LOD	After 2nd LOD	After 3rd LOD	After 4th LOD	After 5th LOD
	1	1·23	0·54	0·73	0·67	0·93	1	13·83	13·72	12·04	10·76	13·26	18·95
	2	1·69	1·42	2·10	2·31	0·90	2	30·23	37·73	39·77	40·70	39·37	40·75
	3	1·84	1·06	0·78	0·77	1·13	3	15·49	18·35	19·57	21·25	22·32	21·64
	4	0·63	0·30	0·35	0·47	0·42	4	24·04	16·80	24·78	22·37	23·16	24·25
	5	1·56	1·56	1·47	1·25	0·74	5	30·89	27·41	29·59	16·01	14·79	37·05
	6	2·05	1·19	0·84	0·63	0·66	6	12·89	13·18	9·30	18·41	18·30	11·23
	7	0·96	1·32	0·69	1·10	1·45	7	59·32	57·43	46·11	35·17	33·92	34·66
	8	0·56	0·53	0·36	0·33	0·45	8	21·70	14·73	12·91	8·21	9·05	10·36
	9	1·86	1·04	1·09	0·97	0·58	9	38·55	33·98	31·46	35·56	34·76	35·64
	10	1·13	0·78	0·48	0·72	2·19	10	24·11	25·38	23·64	19·71	19·06	19·50
							11	10·03	11·63	13·19	16·32	16·47	16·57
Mean		1·35	0·97	0·89	0·92	0·95		25·55	24·58	23·85	22·23	22·22	24·60

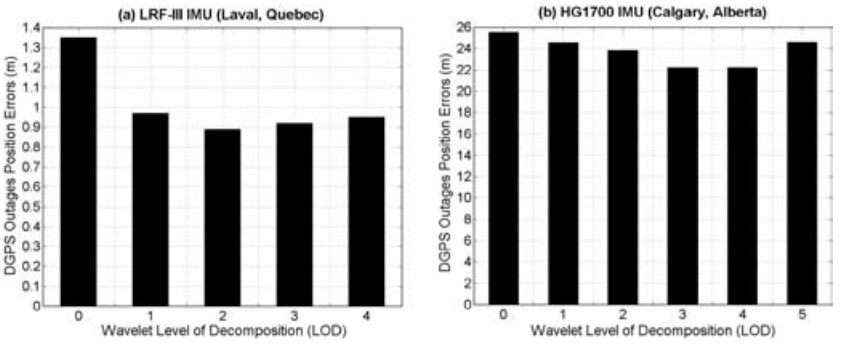

Figure 10. INS Position Errors During DGPS Outages Before and After Wavelet De-noising of Inertial Data.

are not accumulated along the whole trajectory). As a result, INS only positioning is much more affected by the system noise than INS/DGPS positioning during DGPS outages. Consequently, removing or minimizing inertial sensor noise will improve INS stand-alone position errors more than the obtained INS/DGPS position errors during DGPS outages.

6. SUMMARY AND CONCLUSIONS. In this paper, the problem of relatively high measurement noise of inertial sensors in INS stand-alone positioning and INS/DGPS integration applications was discussed. To overcome such a problem, a technique based on wavelet multiple level of decomposition (multi-resolution analysis) was proposed for de-noising inertial sensor data. Wavelet decomposition was chosen since it has the advantage over other signal processing techniques that it is capable of performing signal local analysis and for its ability to reconstruct a signal without loosing any significant information. Wavelet de-noising was applied on two road vehicle inertial data to reduce position errors in INS stand-alone and INS/DGPS applications.

From the work performed in this article, it has been shown that before applying wavelet de-noising of INS sensor kinematic measurements, a frequency analysis must be carried out first for an appropriate choice of the used decomposition level. This technique guarantees the removal of undesirable signal noise and the preservation of the vehicle motion dynamics. Compared to the position errors (RMS) obtained in road vehicle INS kinematic applications (with frequent ZUPTs as updates) using the original INS data, the de-noised INS data results were better by 46%–63%. Using de-noised INS data in INS/DGPS kinematic positioning during DGPS outages, the accumulated position errors at the end of the DGPS outages were reduced by 13%–34%.

REFERENCES

Bruton, A., Schwarz, K. P. and Ŝkaloud, J. (2000). The Use of Wavelets for the Analysis and De-noising of Kinematic Geodetic Measurements. *Proceedings of the IAG Symposia No. 121, Geodesy Beyond 2000: The Challenges of the First Decade*, Birmingham, UK.

https://doi.org/10.1017/S0373463304003005 Published online by Cambridge University Press

Goswami, J. C. and Chan, A. K. (1999). *Fundamentals of Wavelets: Theory, Algorithms and Applications*. John Wiley & Sons Inc.

Keller, W. (2000). *Lecture Notes on Wavelets*. University of Stuttgart, Germany.

Mallat, S. (1998). *A Wavelet Tour of Signal Processing*. Academic Press Limited, USA.

Misiti, M., Misiti, Y., Oppenheim, G. and Poggi, J. M. (2000). *Wavelet Toolbox for the Use with Matlab*. The Math Works Inc., MA, USA.

Nassar, S., Schwarz, K. P., Noureldin, A. and El-Sheimy, N. (2003). Modeling Inertial Sensor Errors Using Autoregressive Models. *Proceedings of the Institute of Navigation* (*ION*) *National Technical Meeting* (NTM 2003), Anaheim, California, USA.

Oppenheim, A. V. and Schafer, R. W. (1999). *Discrete-Time Signal Processing*. Prentice-Hall Inc., Englewood Cliffs, New Jersey, USA.

Polikar, R. (1996). *The Wavelet Tutorial*. Rowan University, College of Engineering Web Server, http://engineering.rowan.edu/~polikar/WAVELETS, Glassboro, New Jersey, USA.

Schwarz, K. P. and Wei, M. (1995). Modeling INS/GPS for Attitude and Gravity Applications. *Proceedings of The 3rd International Workshop of High Precision Navigation*, Stuttgart, Germany.

Ŝkaloud, J. (1999). *Optimizing Georeferencing of Airborne Survey Systems by INS/GPS*. PhD Thesis, Department of Geomatics Engineering, University of Calgary, Calgary, Alberta, Canada, UCGE Report No. 20126.

Strang, G. and Nguyen, T. (1996). *Wavelets and Filter Banks*. Wellesley-Cambridge Press.